Numerical Computation of Space Shuttle Laminar Heating and Surface Streamlines

John V. Rakich*
NASA Ames Research Center, Moffett Field, Calif.

and

Martin J. Lanfranco†
Informatics, Inc., Palo Alto, Calif.

Exact inviscid flowfield codes are used, together with a quasi-three-dimensional boundary-layer analysis, to provide estimates of the windward surface heating and streamline patterns of the shuttle orbiter vehicle under laminar flow conditions. The accuracy and limitations of the methods are established by comparison with available wind-tunnel experiments and with more exact numerical solutions for simple flows. Flight predictions are presented showing the effects of finite-rate (nonequilibrium) chemical reactions, and the effects of varying boundary-layer edge conditions due to the growth of the boundary layer into the inviscid flow (entropy-layer swallowing). Differences between flowfield predictions at wind-tunnel and nominal flight conditions are discussed.

Nomenclature

C_i = concentration of ith chemical species
$\hat{e}_\tau$ = unit vector along the τ coordinate
h = streamline metric or divergence factor
K = inviscid streamline curvature
K_R = correction factor for three-dimensional stagnation heating
k = surface reaction rate
L = body length (32.7 m, full scale)
M = Mach number
N_x, N_r, N_Φ = components of surface normal vector
NO,N,O = nitric oxide, atomic nitrogen, and atomic oxygen
p = pressure
q = heating rate
r = radial distance, cylindrical coordinates
R_N = nose radius
Re = Reynolds number
T = temperature
s,n,t = dimensional streamline, and streamline-normal coordinates
u,v,w = velocity components in either cylindrical, streamline, or boundary-layer coordinates, as indicated by usage
V = total velocity, Eq. (6)
x,y,z = axial, lateral, and vertical distances
α = angle of attack
δ = boundary-layer thickness
ϵ = surface flow angle
θ,ϕ = flow direction angles, Eqs. (16) and (17)
μ = viscosity coefficient
ξ,η,τ = nondimensional streamline and streamline-normal coordinates
ρ = density
Φ = meridional angle, cylindrical coordinates

Subscripts

B = body surface
e = boundary-layer edge
S = shock
δ = quantity evaluated using inviscid properties at the boundary-layer edge
∞ = freestream conditions
0 = stagnation point
2 = conditions behind a normal shock

Presented as Paper 76-464 at the AIAA 11th Thermophysics Conference, San Diego, Calif., July 14-16, 1976; submitted July 30, 1976; revision received Nov. 22, 1976.

Index categories: Boundary Layers and Convective Heat Transfer—Laminar; Reactive Flows; LV/M Aerodynamic Heating.

*Research Scientist. Associate Fellow AIAA.

†Staff Engineer. Member AIAA.

Introduction

AT the outset of the space shuttle program, numerical techniques were not available to determine the entry heating completely for the orbiter vehicle with a single computer code. This necessitated the development of separate inviscid and viscous boundary-layer flow codes in order to provide answers before the first flight. Also, because of the large size of the shuttle orbiter (30 m) and the high-altitude entry trajectory, it was evident that finite-rate chemical reactions needed to be considered in flowfield simulations. Accordingly, the development of three-dimensional (3-D) nonequilibrium inviscid flow codes was initiated, resulting in computer programs reported in Refs. 1-3. The prospects for a fully 3-D boundary-layer code, with nonequilibrium chemistry, seemed, at that time, an improbable development over the span of the shuttle development program. However, there already was available a two-dimensional (2-D) nonequilibrium boundary-layer code,[4] which, by means of the axisymmetric analog,[5-7] could be used to approximate the 3-D shuttle boundary layer. Having the solution of the inviscid flow, one computes the inviscid surface streamlines and the corresponding streamline metric. This information, used in the 2-D boundary-layer code, yields a quasi-3-D boundary-layer solution and heat-transfer prediction. In addition, the corresponding first-order crossflow boundary-layer solution also can be obtained by the methods developed by Fannelop.[8] Thus, by using the exact 3-D inviscid codes with streamline and boundary-layer codes, one can obtain results for flight conditions which reasonably predict the 3-D flowfield over the shuttle.

Two recent papers[9,10] also contribute to the problem of predicting the shuttle heating at flight conditions. Adams et al.[9] used the equivalent axisymmetric body approach and developed correlations for extrapolating wind-tunnel data to flight conditions. Goodrich et al.[10] used substantially the same methods as those described in this paper but considered only equilibrium flight conditions. The present paper emphasizes nonequilibrium flow conditions. The methods used to combine the 3-D inviscid and 2-D boundary-layer solutions

are described, and results obtained for several points on a typical shuttle entry trajectory are presented. Laminar viscous flow is assumed throughout. The accuracy and the limitations of the flowfield methods are established by comparison with experiment and with more exact Navier-Stokes solutions for simple flows.

Heating

Flow Regime and Gas Model

The shuttle orbiter vehicle is expected to enter the atmosphere and experience its peak heating at a high altitude, nominally 80 km, where the boundary layer will be laminar. Some turbulent flow may occur at low altitudes, but turbulence effects are beyond the scope of the present work; laminar flow is assumed for all of the flight conditions studied. For these conditions, it can be shown that boundary-layer displacement effects are small. However, in hypersonic flows the effect of changing edge conditions that are due to boundary-layer growth must be considered. This effect is considered later, in the subsection on "Entropy Layer Swallowing."

Real-gas effects, and particularly finite-rate chemical reactions, appear to be an unknown factor for most of the trajectory. To study these effects, numerical computations are utilized with inviscid and boundary-layer codes which allow for finite-rate (nonequilibrium) chemical reactions. The gas model is a simplified five-species approximation, involving O_2,N_2,NO,O, and N. The details of the model are not given, since they have been described previously in Refs. 1-3. Effects of ionization are neglected in the flow computations, because the electronic contribution to the gas enthalpy is negligible.[3] The equilibrium ionization levels always can be determined from the gas state specified with the present model, if needed for communications or other reasons.

The specific trajectory points, for which detailed results will be presented, are given in Table 1. However, before discussing the flight results, we first describe the theoretical basis for approximating the 3-D viscous boundary-layer flow and then establish the viability of the method by comparison with wind-tunnel data.

Axisymmetric Analog

Although computational 3-D boundary-layer methods have received much attention recently, adequate computer codes were not available at the start of the present study. Therefore, the 2-D analog method, initially developed by Cooke[5] and later extended by DeJarnette,[7] was adopted. The essence of the method lies in the application of the axisymmetric form of the boundary-layer equations along the inviscid surface streamlines, with the axisymmetric radius replaced by the inviscid streamline metric.

To outline the procedure, let s,n,t be dimensional distances in orthogonal streamline coordinates, and let ξ,η,τ be generalized coordinates satisfying the differential relations

$$ds=h_1 d\xi \quad dn=h_2 d\eta \quad dt=h_3 d\tau \tag{1}$$

where the factor h_3 is the "streamline metric" used in the axisymmetric analog. Since h_1 and h_2 are not needed in the present analysis, h_3 can be denoted by h. Given the inviscid velocity components u,v,w and the body radius r as functions of x and Φ, the streamlines and the metric are determined by a numerical solution of the following differential equations.

$$\left(\frac{\partial \Phi}{\partial x}\right)_\tau = \frac{w}{ru} \tag{2}$$

$$\left(\frac{\partial F}{\partial x}\right)_\Phi = F\left(\frac{\partial G}{\partial \Phi}\right)_x - G\left(\frac{\partial F}{\partial \Phi}\right)_x \tag{3}$$

where the subscripts indicate the coordinate held constant. The terms in Eq. (3) are defined by

$$G=w/ru \tag{4}$$

$$F=\frac{hV}{ru}\left[1+\left(\frac{\partial r}{\partial x}\right)^2+\frac{1}{r^2}\left(\frac{\partial r}{\partial \Phi}\right)^2\right]^{-1/2} \tag{5}$$

$$V=(u^2+v^2+w^2)^{1/2} \tag{6}$$

Further details on the procedures of the computation are given in Refs. 6 and 11.

With the metric h determined in this way, and with the remaining inviscid edge conditions, pressure and entropy, a viscous boundary-layer calculation can be made. For the present work, the computer code described by Tong et al.[4] has been used. This boundary-layer code includes equilibrium or finite-rate chemical reactions that are central to the problem of shuttle-flight heating predictions.

Table 1 Conditions for nominal shuttle flight trajectory 14414

Velocity km/sec	Velocity kft/sec	Altitude km	Altitude kft	Angle of attack, deg
7.955	26.1	83.82	275	40.0
7.620	25.0	74.98	246	41.4
6.614	21.7	68.88	226	40.2
5.944	19.5	64.92	213	34.5
5.121	16.8	60.66	199	31.8
3.886	12.75	53.34	175	31.0

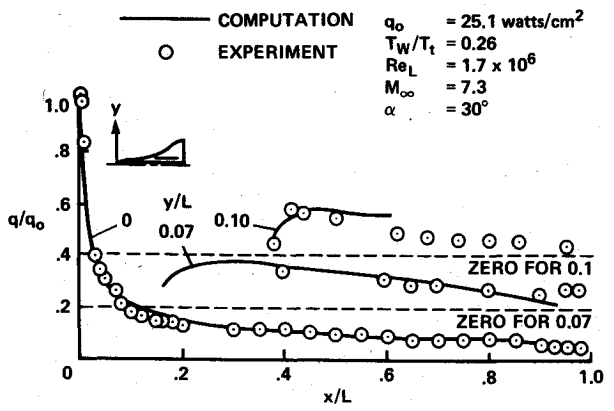

Fig. 1 Shuttle windward surface heating for wind-tunnel conditions.

Wind-Tunnel Data

In order to verify the theoretical methods just described, numerical results are compared with available experimental data. Figure 1 shows data obtained in the Ames 3.5-ft hypersonic wind tunnel[12] at $M=7.3$ and 30° angle of attack. Data and calculations are presented for the windward centerline and two other windward spanwise stations. The agreement is very good except for the outboard station, $y/L=0.1$. The numerical result goes only to about $x/L=0.6$ on the outboard station because the inviscid solution for the wing was not modeled accurately in the inviscid program. It was necessary to increase the wing sweep angle in order to get the inviscid program[1] to calculate past $x/L=0.6$. This may perturb the heating results shown for $x/L>0.6$, although it is felt that the effect is small.

On the centerline at $0.1<x/L<0.2$, the experiment is slightly lower than the calculation. This may be due to conduction effects in the experiment or to a local breakdown in the analog theory. Fannelop[8] shows, for a blunt cone, that the analog tends to predict a higher heating in the region just downstream of the blunt nose. Also, the present calculations have not accounted for the effect of boundary-layer thickness

on the inviscid streamlines. Including this effect likely would decrease the streamline metric and the corresponding heating prediction. This discrepancy, however, is not large, and Fig. 1 suggests that the present analog theory is a viable one for the shuttle.

The reference heating, q_0 in Fig. 1, is the value calculated for a sphere. (The full-size spherical cap has a 2⅓-ft, 0.71-m radius, and the model is 0.0175 scale.) In actuality, the stagnation point probably is off the spherical cap at 30° angle of attack, but the experimental data suggest that the effect is not large. However, at larger angles of attack the stagnation point will move farther from the spherical cap, and three-dimensional effects may become important. An estimate of this effect is studied next.

Three-Dimensional Stagnation Point

Since the stagnation region of the shuttle is inherently three-dimensional, some correction must be made to the two-dimensional analog theory. As presently formulated, a match point is selected a short distance from the true stagnation point, where the streamline calculation originates. Upstream from the match point on each streamline, it is assumed that a spherical nose exists which is tangent to the true body. This spherical nose is assumed to support a Newtonian pressure distribution, which then permits calculation of a 2-D boundary-layer solution. The heating for the matched sphere is higher than for the real shape because of the smaller axial radius of curvature of the sphere.

Reshotko[13] has shown that the heating to a three-dimensional stagnation point is related to the two-dimensional value in a simple geometrical manner.‡ Assuming a Newtonian pressure distribution, one can write

$$q_{3D} = K_R q_{\text{sphere}} \tag{7}$$

where

$$K_R = \{ [1 + (R_\Phi / R_x)] (R_N / 2R_\Phi) \}^{1/2} \tag{8}$$

and where R_x and R_Φ are the radii of curvature in the axial and transverse directions, and R_N is the radius of the spherical nose. Goodrich et al.[10] have employed a similar correction in a form based on the stagnation-point velocity gradients. The results should be similar, except that the velocity gradients will be more dependent on the accuracy of the blunt-body solution.

The radii of curvature, R_x and R_Φ, depend on the location of the stagnation point, which, at high Mach numbers, is primarily a function of angle of attack. Using typical flowfield solutions to determine the stagnation-point location, assuming dependence on angle of attack only, the correction factor $K_R = 1 - 0.0067(\alpha - 26)$ for $30 < \alpha < 42$ is obtained. The 3-D correction is only about 3% at 30° angle of attack but increases to about 10% at 40°.

Flight Stagnation Heating

Having verified the computational method by comparison with experiment, the computations can be applied to the actual shuttle flight conditions. Flight conditions are difficult, if not impossible, to simulate experimentally, especially when chemical reactions are involved. Numerical computations, on the other hand, are not so limited.

Figure 2 shows the predicted shuttle stagnation-point heating calculated for a sphere and with the correction factor for 3-D effects applied. Shown are results of boundary-layer calculations with equilibrium and finite-rate (nonequilibrium) chemical reactions. In the peak heating region, the nonequilibrium heating rates range from 10 to 20% below the equilibrium values, with the larger differences at higher velocities and altitudes (see Table 1 for corresponding altitudes). For both cases, equilibrium inviscid flow conditions are set at the boundary-layer edge. Also shown for comparison is the approximate empirical method due to Fay and Riddell,[14] evaluated using equilibrium conditions, unit Lewis number, and the Sutherland viscosity relation. The Fay and Riddell result is almost the average of the present equilibrium and reacting calculations.

‡Note that Eqs. (18) and (19) of Ref. 13 incorrectly indicate a one-half power relationship between the velocity gradient and radius of curvature instead of the correct linear dependence, which is well known.[14]

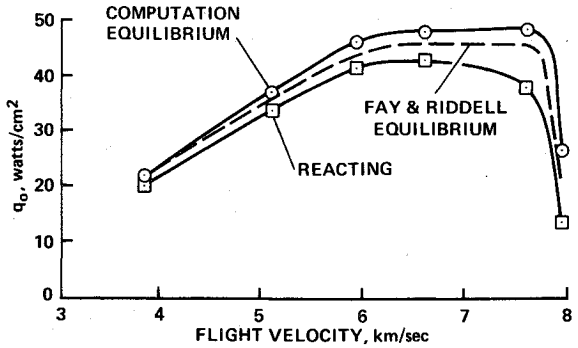

Fig. 2 Predicted flight stagnation heating; trajectory 14414 (Table 1).

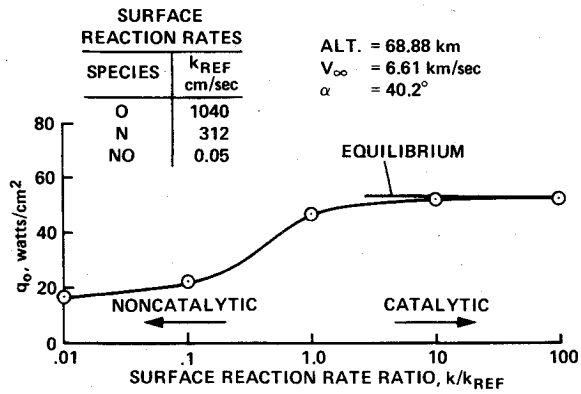

Fig. 3 Predicted shuttle stagnation heating with varying surface reaction rates.

The heating calculated for finite-rate chemical reactions is critically dependent on surface catalytic efficiency. This catalytic efficiency is specified in the calculation in terms of species reaction rates in the presence of the surface, that is, surface reaction rates. The nominal or reference values used for the present are based on limited experimental data[4,15] obtained with the shuttle heat-shield material. These nominal surface reaction rates are listed in Fig. 3, which also shows the effect on heating of variations from 0.01 to 100 times the nominal values. It can be seen that the nominal values are near the equilibrium (catalytic wall) limit, and that a significant reduction in heating would result if a noncatalytic surface were attainable.

Flight Afterbody Heating

The flight heating on the windward centerline, with both finite-rate and equilibrium chemical reactions, has been examined. However, before looking at the results, the manner in which the boundary-layer edge conditions are set must be explained.

First, since the present inviscid solution was performed only for nonequilibrium chemistry, an assumption was necessary to obtain equilibrium heating. It is well known that the surface pressure is rather insensitive to the reaction rates. It therefore was assumed that the same inviscid pressure distribution applied to equilibrium and nonequilibrium flows. For equilibrium flow, the inviscid pressure and entropy completely determine the boundary-layer edge conditions.

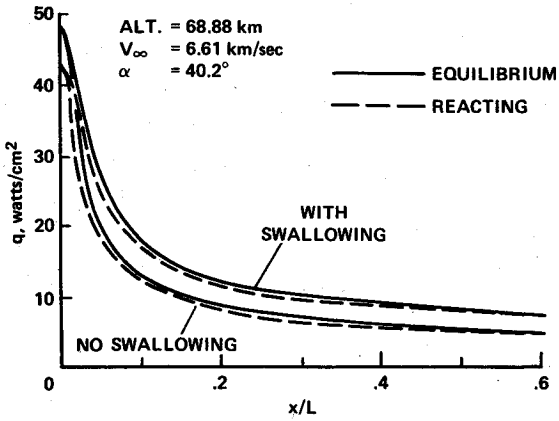

Fig. 4 Calculated windward centerline heating for flight conditions.

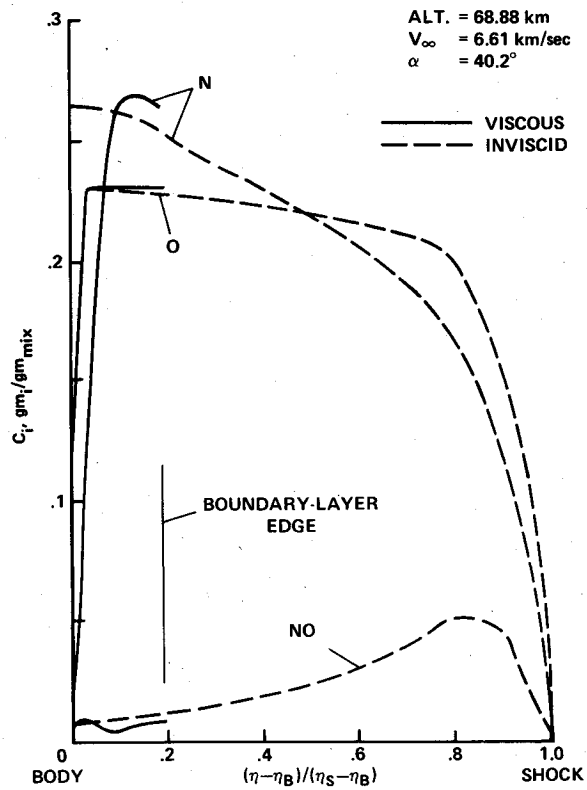

Fig. 5 Boundary- and shock-layer species profiles: stagnation point.

The entropy may be constant or may vary, depending on whether the boundary-layer thickness is taken into account.

Second, for nonequilibrium flow, the species concentrations must be specified. For the case where the boundary-layer thickness is negligible, it is argued that the inviscid blunt-body flow will be nearly in equilibrium at the body surface. (This assumption is necessary because the finite-volume method[2] does not calculate surface properties. The approximation was found to be reasonable in calculations with the method of characteristics.[1]) When a finite boundary-layer thickness was allowed, the inviscid values of pressure, entropy, and species concentrations were used to determine the edge conditions.

Figure 4 shows the heating predicted by the methods just described. Two sets of curves are shown, with the lower set (no swallowing) obtained by using inviscid conditions evaluated under the assumption of zero boundary-layer thickness. The upper set (with swallowing) accounts for the finite thickness of the boundary layer and is discussed in the next subsection. As regards nonequilibrium effects, it appears that the effect of finite-rate chemical reactions become negligible some distance behind the nose. Even though the inviscid flow may be far out of equilibrium, the surface catalytic effects in the boundary layer tend to drive the flow toward equilibrium. However, this conclusion is based on the best current estimate of surface reaction rates for which there is not a great deal of data.[15] The conclusion could change, as indicated in Fig. 5, if the surface reaction rates are lower.

Entropy-Layer Swallowing

It has been known for some time that the blunt-nose entropy layer has a strong effect on boundary-layer edge properties (see, for example, Mayne[16] or Adams et al.[17]). As the boundary layer on a long blunted body grows, the gas that passed through the blunt-body shock is entrained in the viscous layer, and the boundary-layer edge conditions change to those corresponding to an oblique shock. This is called entropy-layer swallowing.

To include swallowing, one must determine the boundary-layer edge conditions from the inviscid solution at a distance δ above the wall. This presently is done by successive approximations. In the first approximation, the boundary-layer edge conditions are taken at the wall, $\delta = 0$, and the calculated δ is used in subsequent trails. Three trials usually suffice to converge on the proper conditions. The inviscid solution remains unchanged in this process; that is, boundary-layer displacement effects are neglected.

Near the stagnation point, the inviscid gradients are not large, and so the swallowing effects are not very large there. To illustrate this point, Fig. 5 shows the inviscid and viscous profiles of chemical species across the shock layer. Downstream from the nose cap, the entropy layer thins out, and large gradients in the inviscid flow develop. This situation is illustrated by the velocity distributions in Fig. 6. When using the inviscid wall conditions, there is a large discrepancy between the viscous and inviscid velocities at the edge of the boundary layer. The mismatch gets worse with increasing distance from the nose.

In the course of the present investigation, it became apparent that the effect of swallowing on heating was not the same at wind-tunnel and flight conditions. Therefore, there is a need to look at aerodynamic heating theory to explain the effects of swallowing. Following the theory of Lees,[18] the heating distribution is given as follows, with the axisymmetric radius r replaced by the streamline metric h.

$$\frac{q}{q_0} = \frac{0.5(p/p_0)(u_e/u_\infty)hR_N^{1/2}}{[\int_0^s (p/p_0)(u_e/u_\infty)h^2 d\xi]^{1/2}[(1/u_\infty)(du_e/d\theta)_0]^{1/2}} \quad (9)$$

Equation (9) is the result of many simplifying assumptions that make it independent of the Reynolds number. Nevertheless, experience has shown that the Lees theory predicts the

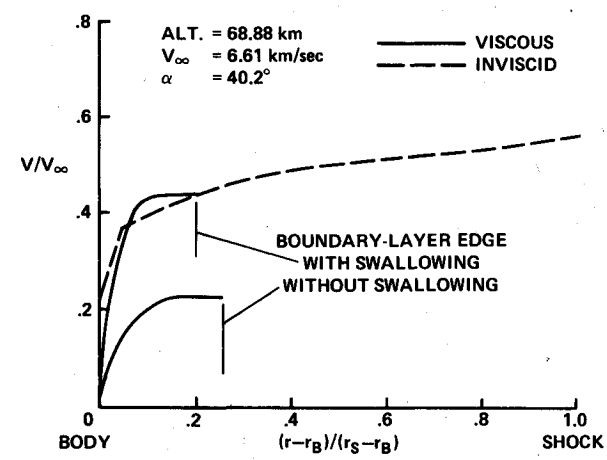

Fig. 6 Boundary- and shock-layer velocity profiles: $x/L = 0.047$.

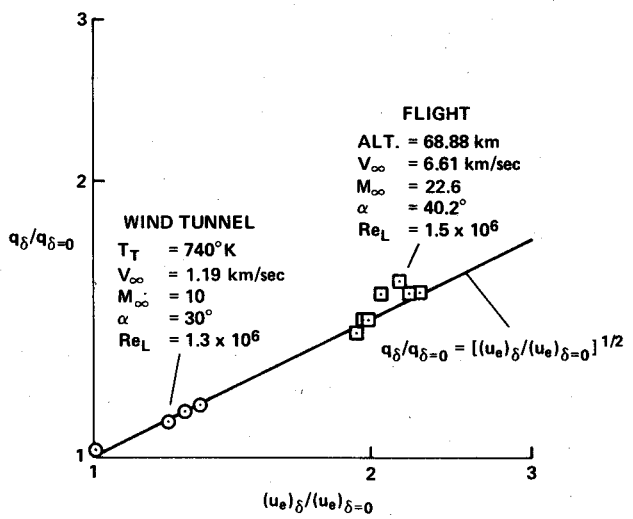

Fig. 7 Correlation of boundary-layer swallowing effects on heating.

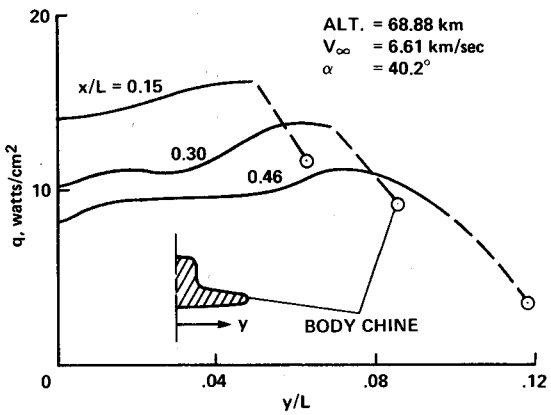

Fig. 8 Calculated windward spanwise heating for equilibrium flight conditions including swallowing effects.

dominant trends very well. Using this theory, the heating is found to vary as the one-half power of the velocity

$$q_\delta/q_{\delta=0} = [(u_e)_\delta/(u_e)_{\delta=0}]^{1/2} \tag{10}$$

where the subscripts δ and $\delta=0$ denote the *inviscid* properties at the boundary-layer edge and at the wall.

Figure 7 shows the heating ratio calculated with the flowfield codes for both flight and wind-tunnel conditions; the flight case is for equilibrium chemistry. Although there are some local deviations from the trend predicted by Eq. (10), the overall dependence of the wind-tunnel and flight computations unmistakably follows the half-power law. Even though the edge Mach and Reynolds numbers are changed by swallowing, it is the velocity ratio alone that correlates the heating. The velocity ratio is much larger at flight because of the effects of molecular dissociation on the edge velocity.

Figure 7 explains why good agreement was obtained with the experimental data in Fig. 2, even though swallowing was neglected. For wind-tunnel conditions, the heating ratio in Fig. 7 is less than 1.15, and, therefore, the effect of swallowing is within normal experimental and computational uncertainties. At flight conditions, however, the effect is appreciable and must be included.

Shown in Fig. 4 are the flight heating predictions, including the effects of swallowing for both equilibrium and reacting flow. Both curves are affected equally by swallowing, and so the conclusion still holds that nonequilibrium effects do not change the heating downstream from the nose cap appreciably.

Off-Centerline Heating

In the comparison with wind-tunnel data (Fig. 1), it was shown that the present numerical method gave reasonable results away from the symmetry plane. Figure 8 shows windward spanwise heating distributions for the flight case. These predictions include the entropy swallowing, which has a nearly uniform effect across the span. Three axial stations are shown in Fig. 8. The forward station, $x/L=0.15$, has a heating distribution typical of elliptic cross section bodies. The other stations, $x/L=0.30$ and 0.46, have a peculiar dip near the centerline, the reason for which is not clear at this time. In order to get a more complete picture of the 3-D viscous flow away from the centerline and to estimate the error in the heating results there, it is necessary to consider the next level of approximation.

Crossflow and Streamlines

Crossflow Theory

Fannelop[8] solved the three-dimensional boundary-layer equations by a systematic perturbation procedure. The first approximation is the axisymmetric analog described in a previous section of this paper. A perturbation procedure then is proposed in terms of a parameter K, the curvature of the inviscid-surface streamlines. The first-order perturbation of the crossflow velocity turns out to be independent of the other velocity components and can be determined directly from the crossflow momentum equation. This equation is

$$\frac{\partial}{\partial n}\left(\mu\frac{\partial w_1}{\partial n}\right) - \rho v\frac{\partial w_1}{\partial n} - \rho u\frac{\partial w_1}{\partial s} - \left(\frac{\rho u}{h}\frac{\mathrm{d}h}{\mathrm{d}s}\right) w_1$$

$$= K\rho u_e{}^2\left(\frac{\rho_e}{\rho} - \frac{u^2}{u_e{}^2}\right) \tag{11}$$

where s is the inviscid streamline and n is the surface normal direction, and where ρ, u, v and μ are known functions of (s,n) from the 2-D analog solution. The dependent variable w_1 is the first-order perturbation in the crossflow velocity, in streamline coordinates. The forcing function on the right side of Eq. (11) is proportional to K, the inviscid streamline curvature. If $K=0$ everywhere, the flow remains 2-D; but if $K\neq 0$ anywhere, then there will be a w_1, and the flow is 3-D.

The streamline transverse curvature or, more properly, the geodesic curvature of the surface $\tau=$ const is related to the pressure gradient by

$$K = (1/\rho V^2)\,\hat{e}_\tau\cdot\nabla p \equiv (1/\rho V^2 h)\,(\partial p/\partial\tau) \tag{12}$$

Using the intrinsic flow equations,[19] the following expression for curvature in terms of the inviscid flow angles is obtained.

$$K = \sin\delta\left(\frac{\sin^2\phi\cos\theta}{r} - \cos\theta\frac{\partial\theta}{\partial s}\right) - \cos\delta\left(\frac{\sin\phi\sin\theta}{r} + \frac{\partial\phi}{\partial s}\right) \tag{13}$$

where

$$\delta = \cos^{-1}(N_r\cos\theta - N_x\sin\theta) \tag{14}$$

$$\{N_x, N_r, N_\Phi\} = \frac{[-r_x, 1, -(1/r)r_\Phi]}{\{1+r_x^2+[(1/r)r_\Phi]^2\}^{1/2}} \tag{15}$$

The flow angles θ and ϕ are related to the cylindrical velocity components[19] u, v, w by

$$\theta = \tan^{-1}(v/u) \tag{16}$$

$$\phi = \tan^{-1}[w/(u^2+v^2)^{1/2}] \tag{17}$$

Solution of the Crossflow Equations

Since w_1 is defined relative to the inviscid streamline, it vanishes at the outer edge of the boundary layer. Therefore,

the boundary conditions for Eq. (11) are

$$w_1(0) = w_1(n_e) = 0 \tag{18}$$

A finite-difference solution of Eq. (11) is obtained in a routine manner by employing the Crank-Nicholson difference scheme and a standard tridiagonal matrix inversion. The equation is linear, but the coefficients are variable functions of ξ and η, which are obtained from three other computer programs. These programs are 1) the inviscid flowfield code,[1-3] 2) the streamline metric code,[11] and 3) the axisymmetric boundary-layer code.[4] Data transfer is made by means of a magnetic storage device.

Solution for the Viscous Streamlines

The direction of the viscous streamlines, relative to the inviscid flow, is given by

$$\epsilon_v(n) = \tan^{-1}(w_1/u) \tag{19}$$

which has the limiting value at $n = 0$

$$\epsilon_v(0) = \tan^{-1}\left(\frac{\partial w_1}{\partial n} \Big/ \frac{\partial u}{\partial n}\right)_w \tag{20}$$

The inviscid stream angle can be shown to be

$$\sin\epsilon_i = \frac{N_\Phi[\cos\phi\sin\theta + (N_x/N_r)\cos\phi\cos\theta]}{[1+(N_x/N_r)^2]^{1/2}} - N_r[1+(N_x/N_r)^2]^{1/2}\sin\phi \tag{21}$$

where the terms are defined in Eqs. (15-17), and the total angle is

$$\epsilon = \epsilon_i + \epsilon_v \tag{22}$$

Here, ϵ is measured from the line of intersection of the body surface and the cylindrical-coordinate plane $\Phi = \text{const}$.

To solve for the streamline path, write the following differential relation, in analogy to the inviscid streamlines.[6]

$$d\Phi = (W/rU)\,dx \tag{23}$$

except that here W and U are fictitious velocities related to the surface stream angle by

$$W = \frac{\sin\epsilon}{N_r[1+N_\Phi^2/(N_x^2+N_r^2)]\,[1+(N_x/N_r)^2]^{1/2}} \tag{24}$$

$$U = \frac{N_x N_\Phi W}{(N_x^2+N_r^2)} + \left\{\frac{1-W^2[1+(N_\Phi/N_r)^2]}{[1+(N_x/N_r)^2]} + \left[\frac{N_x N_\Phi W}{N_x^2+N_r^2}\right]^2\right\}^{1/2} \tag{25}$$

The sign convention used in Eq. (23) is one in which Φ is measured from the windward plane of symmetry. Now all of the information needed to integrate Eq. (23) is available, starting from an initial position $\Phi = \Phi_0$ at $x = x_0$.

Crossflow Boundary Layer on a Blunt Cone

Since there are no really adequate experimental data to verify the small crossflow solution, more exact numerical results for a simple shape are used. Lubard and Rakich[20] have applied a numerical method that utilizes the parabolic Navier-Stokes (PNS) equations for a blunt cone. The method solves the three-dimensional steady-flow equations in the entire flow region from body to shock, neglecting only the streamwise second derivatives (see Ref. 20 for details). The method has been checked against experimental heating and flowfield measurements and gives excellent results. In respect to the present approximate method, the PNS solution may be taken as exact.

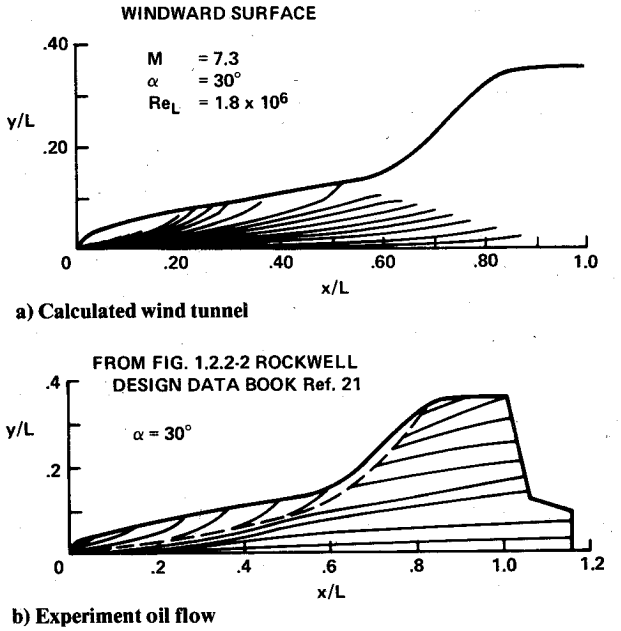

Fig. 9 Viscous streamlines on shuttle windward side.

By comparing the present method with the PNS solution for a blunt cone, it has been possible to obtain a correlation of the error in terms of the average streamline curvature

$$\bar{K} = \frac{R_N}{s}\int_0^s K(\xi)\,d\xi \tag{26}$$

This form was chosen because the error must depend on the curvature, and there must be some effect of the history of the streamline. It was found that, for a mean curvature less than about 0.15 in magnitude, the stream angle error will be less than about 5°. This fact will be used to estimate the error for the shuttle, for which the more exact PNS method has not been applied.

Shuttle Crossflow and Streamlines

The streamline tracing methods just described were applied to the shuttle geometry, both for wind-tunnel and flight conditions. Figures 9a and 9b show the calculated streamlines and wind-tunnel oil-streak experiments, as interpreted by designers.[21] It is seen that the calculated streamlines have the same essential features as the experiment. These calculations were made without taking into account swallowing effects on the inviscid streamlines, and this effect may reduce stream angles slightly. The calculated streamlines do not extend onto the wing, because the inviscid flow computation failed in the region where the bow shock intersects the secondary shock from the wing root. Therefore, the computations typically are terminated at about $x/L = 0.6$. In the wind-tunnel case, however, the wing sweep was modified to allow the calculation to proceed farther downstream. Therefore, the streamlines may show too much spreading for $x/L > 0.6$, although it is felt that the error is small for the region shown.

The motivation for finding the streamlines is to permit heat-shield tile gaps to be misaligned purposely with the streamlines; otherwise high heating can occur in the gaps. For flight conditions, the calculated streamlines are shown in Fig. 10. The pattern is substantially the same as in the wind-tunnel case, with the exception of the body edge or chine.

The reason for the difference between the calculated wind-tunnel and flight streamlines near the chine is not entirely

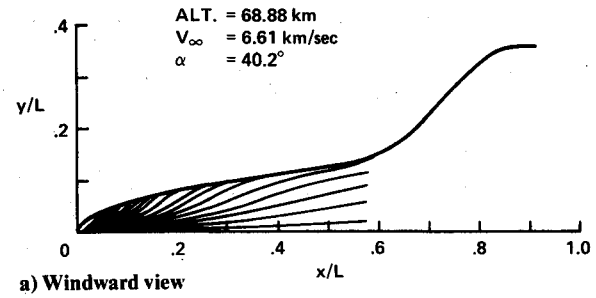

a) Windward view

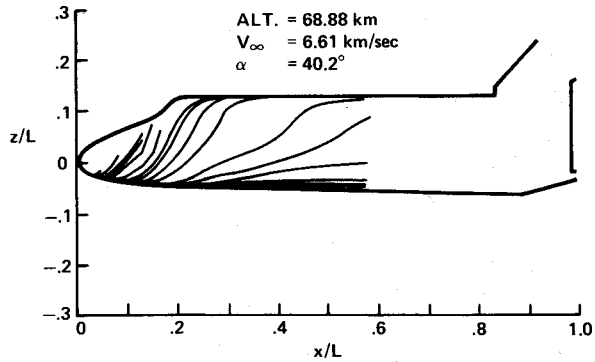

b) Side view

Fig. 10 Calculated viscous streamlines for flight conditions.

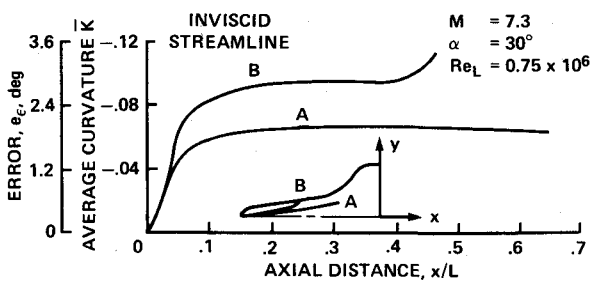

Fig. 11 Estimated error in viscous stream angles.

clear. It is clear, however, that the accuracy of the present method begins to break down near the chine. Figure 11 shows an error estimate based on the mean curvature given by Eq. (26). It is seen that the estimated error in the stream angle is less than 3°, except near the chine. The error rises rapidly in that region, and, therefore, the results should be used with caution in that region. This word of caution about the chine region also applies to the heating predictions in Fig. 8. On the other hand, Fig. 11 indicates that the method should give good results over most of the windward side of the shuttle, even at 40° angle of attack.

Concluding Remarks

Exact inviscid flowfield codes have been used, together with a 2-D boundary-layer code and quasi-3-D theories, to provide estimates of the heating and streamline patterns on the space shuttle orbiter. The results of the flowfield codes have been checked against wind-tunnel experiment and more exact theories to establish their accuracy and limitations. Since the flowfield codes can be applied to flight conditions as well as to wind-tunnel conditions, it is felt that they correctly predict the shuttle-flight heating to the same general accuracy that they predict the wind-tunnel case.

It was found, however, that blunt-body entropy-layer effects are likely to be significant at flight conditions, whereas they are nearly negligible for laminar flow at wind-tunnel conditions. Using the best current estimates of catalytic surface reaction rates, nonequilibrium chemical effects result in only about 10-20% decrease in heating in the stagnation regions and have a negligible effect elsewhere on the windward side.

Numerical solutions of the small crossflow momentum equation were used to predict the viscous surface streamlines. An error estimation in terms of the inviscid streamline curvature was developed. Based on this criterion, it was estimated that the method would yield surface stream angles to within 3° on the windward side of the shuttle in regions away from the chine, where the body curvature is not great. The method is not considered applicable to the leeward side of the body under conditions where separated flow and vortices are present.

Finally, it should be mentioned again that an approximate 3-D method was developed in order to make a timely impact on the shuttle development program, and it is not intended to supplant more exact numerical methods that are now in preparation. However, until such methods become operational, the present technique provides a more rational way to predict flight conditions than simple extrapolation of wind-tunnel data.

References

[1]Rakich, J. V. and Park, C., "Nonequilibrium Three-Dimensional Supersonic Flow Computations with Application to the Space Shuttle Orbiter Design," *Proceedings of the Symposium on Application of Computers to Fluid Dynamic Analysis and Design,* Polytechnic Institute of Brooklyn Graduate Center, Farmingdale, N. Y., Jan. 1973.

[2]Rizzi, A. and Bailey, H., "Reacting Nonequilibrium Flow Around the Space Shuttle Using a Time Split Method," NASA SP 347, 1975.

[3]Rakich, J. V., Bailey, H. E., and Park, C., "Computation of Nonequilibrium Three-Dimensional Inviscid Flow Over Blunt-Nosed Bodies Flying at Supersonic Speeds," AIAA Paper 75-835, 8th Fluid and Plasma Dynamics Conference, Hartford, Conn., 1975.

[4]Tong, H., Buckingham, A. C., and Curry, D. M., "Computational Procedure for Evaluations of Space Shuttle TPS Requirements," AIAA Paper 74-518, 7th Fluid and Plasma Dynamics Conference, Palo Alto, Calif., 1974.

[5]Cooke, J. C., "An Axially Symmetric Analogue for General Three-Dimensional Boundary Layers," British Aeronautical Research Council, R&M 3200, 1961.

[6]Rakich, J. V. and Mateer, G. G., "Calculation of Metric Coefficients for Streamline Coordinates," *AIAA Journal*, Vol. 10, Nov. 1972, pp. 1538-1540.

[7]DeJarnette, F. R. and Hamilton, H. H., "Inviscid Surface Streamlines and Heat Transfer on Shuttle-Type Configurations," *Journal of Spacecraft and Rockets,* Vol. 10, May 1973, pp. 314-321.

[8]Fannelop, T. K., "A Method of Solving the Three-Dimensional Laminar Boundary-Layer Equations with Application to a Lifting Re-Entry Body," *AIAA Journal*, Vol. 6, June 1968, pp. 1075-1084.

[9]Adams, J. C. Jr., Martindale, W. R., Mayne, A. W. Jr., and Marchand, E. O., "Real Gas Scale Effects on Shuttle Orbiter Laminar Boundary-Layer Parameters," *Journal of Spacecraft and Rockets,* Vol. 14, May 1977, pp. 273-279.

[10]Goodrich, W. D., Li, C. P., Houston, C. K., Chiu, P., and Olmedo, L., "Numerical Computations of Orbiter Flow Fields and Laminar Heating Rates," *Journal of Spacecraft and Rockets,* Vol. 14, May 1977, pp. 257-264.

[11]Rakich, J. V. and Pegot, E. B., "Flow Field and Heating on the Windward Side of the Space Shuttle Orbiter," NASA SP 347, 1975.

[12]Cummings, J. W. and Lockman, W. K., "Aerodynamic Heating Results for a Space Shuttle Orbiter 140B Model in the NASA/Ames 3.5-Foot Hypersonic Wind Tunnel (Test OH26)," Chrysler Corp., New Orleans, La., DMS-DR-2193.

[13]Reshotko, E., "Heat Transfer to a General Three-Dimensional Stagnation Point," *Jet Propulsion*, Vol. 28, Jan. 1958, pp. 58-60.

[14]Fay, J. A. and Riddell, F. R., "Theory of Stagnation Point Heat Transfer in Dissociated Air," *Journal of the Aeronautical Sciences*, Vol. 25, Feb. 1958, pp. 73-85.

[15]Schaefer, J. W., Tong, H., Clark, K. J., Shusland, K. E., and Neuner, G., "Analytic and Experimental Evaluation of Flowing Air Test Conditions for Selected Metallics in a Shuttle TPS Application," NASA CR 2531, 1975.

[16]Mayne, A. W. Jr., "Calculation of the Boundary-Layer Flow in the Windward Plane of a Spherically Blunted Axisymmetric Body at Angle of Attack, Including Streamline-Swallowing Effects," Arnold Engineering Development Center, AFS, Tenn.,AEDC-TR-73-166, 1973.

[17]Adams, J. C. Jr., Martindale, W. R., Mayne, A. W. Jr., and Marchand, E. O., "Real Gas Scale Effects on Hypersonic Laminar Boundary-Layer Parameters Including Effects of Entropy Layer Swallowing," Arnold Engineering Development Center, AFS, Tenn., AEDC-TR-72-2, Dec. 1975.

[18]Lees, L., "Laminar Heat Transfer Over Blunt-Nosed Bodies at Hypersonic Flight Speeds," *Jet Propulsion*, Vol. 26, April 1956, pp. 259-269.

[19]Rakich, J. V., "A Method of Characteristics for Steady Three-Dimensional Supersonic Flow with Application to Inclined Bodies of Revolution," NASA TN D-5341, 1969.

[20]Lubard, S. C. and Rakich, J. V., "Calculation of the Flow on a Blunted Cone at a High Angle of Attack," AIAA Paper 75-149, 13th Aerospace Sciences Meeting, Pasadena, Calif., 1975.

[21]"Space Shuttle Orbiter Entry Aerodynamic Heating Data Book," Rockwell International Space Division, Downey, Calif., SD73-SH-0184A, July 1975.

From the AIAA Progress in Astronautics and Aeronautics Series

AERODYNAMICS OF BASE COMBUSTION—v. 40

Edited by S.N.B. Murthy and J.R. Osborn, Purdue University, A.W. Barrows and J.R. Ward, Ballistics Research Laboratories

It is generally the objective of the designer of a moving vehicle to reduce the base drag—that is, to raise the base pressure to a value as close as possible to the freestream pressure. The most direct and obvious method of achieving this is to shape the body appropriately—for example, through boattailing or by introducing attachments. However, it is not feasible in all cases to make such geometrical changes, and then one may consider the possibility of injecting a fluid into the base region to raise the base pressure. This book is especially devoted to a study of the various aspects of base flow control through injection and combustion in the base region.

The determination of an optimal scheme of injection and combustion for reducing base drag requires an examination of the total flowfield, including the effects of Reynolds number and Mach number, and requires also a knowledge of the burning characteristics of the fuels that may be used for this purpose. The location of injection is also an important parameter, especially when there is combustion. There is engineering interest both in injection through the base and injection upstream of the base corner. Combustion upstream of the base corner is commonly referred to as external combustion. This book deals with both base and external combustion under small and large injection conditions.

The problem of base pressure control through the use of a properly placed combustion source requires background knowledge of both the fluid mechanics of wakes and base flows and the combustion characteristics of high-energy fuels such as powdered metals. The first paper in this volume is an extensive review of the fluid-mechanical literature on wakes and base flows, which may serve as a guide to the reader in his study of this aspect of the base pressure control problem.

522 pp., 6x9, illus. $19.00 Mem. $35.00 List

TO ORDER WRITE: Publications Dept., AIAA, 1290 Avenue of the Americas, New York, N. Y. 10019